HiSST: 3rd International Conference on
High-Speed Vehicle Science Technology
14 -19 April 2024, Busan, Korea

Design and Objectives of the Air-breathing Propulsion Experiment Technology Demonstrator (APEX-TD)

Johannes Riehmer[1], Florian Klingenberg[1], Thomas Röhr[2], Christian Zuber[3], Christian Schnepf[4] and Ali Gülhan[1]

Abstract

Ramjets and Scramjets have the potential to be the next generation alternatives for high-speed flight and access-to-space with air-breathing propulsion system. APEX-TD is a DLR low-cost flight experiment designed to investigate essential technologies for afore mentioned propulsion concepts and provide real flight data for verification of numerical simulations and experiment data. The flight was launched on-top of a single-stage Red Kite sounding rocket during its qualification flight on November 13, 2023 in Andøya, Norway.

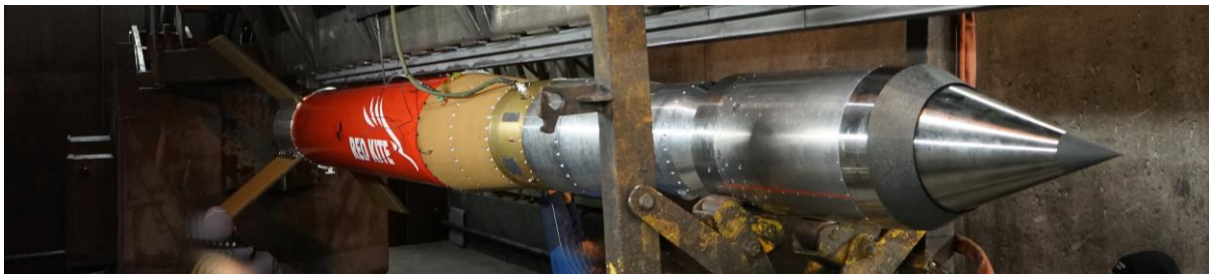

The main characteristic of the experiment is a supersonic axial-symmetric inlet with internal flow path and an active starting mechanism for a design Mach number of 5. During the flight a maximal Mach number of 4.8 was reached. As key technologies for scramjet combustion 3D printed looped strut injectors with nitrogen injection were tested. Further features were ceramic structures integrated in vehicle components with high aerothermal loads and a dedicated instrumentation of the external and internal flow path.

This paper gives an overview of the vehicle design concept, experimental set-up and configuration as well as scientific objectives of the APEX-TD experiment in general. It also provides results of first analysis of the flight trajectory and scientific data collected during the flight.

Keywords: *flight experiment, inlet, supersonic, scramjet*

[1] DLR, Institute of Aerodynamics and Flow Technology – Supersonic and Hypersonic Technologies, Linder Hoehe, 51147 Cologne, Germany, johannes.riehmer@dlr.de, florian.klingenberg@dlr.de, ali.guelhan@dlr.de
[2] DLR, Space Operations and Astronaut Training – Mobile Rocket Base, Muenchener Str. 20, 802234 Wessling, Germany, thomas.roehr@dlr.de
[3] DLR, Institute of Structures and Design – Space System Integration, Pfaffenwaldring 38-40, 70569 Stuttgart, Germany, christian.zuber@dlr.de
[4] DLR, Institute of Aerodynamics and Flow Technology – High Speed Configurations, Bunsenstr. 10, 37073 Goettingen, Germany, christian.schnepf@dlr.de

Nomenclature

AEDB	Aerodynamic Database
AoA	Angle of Attack
APEX-TD	Air-breathing Propuulsion Experiment
CAD	Computer Aided Design
CFD	Computation Fluid Dynamics
COG	Center of Gravity
CP	Center of Pressure
CR	Contraction Ratio
DAQ	Data Acquisition
DLR	German Aerospace Center
FEM	Finite Element Method
M	Mach number
MCR	Mass Capture Ratio
RANS	Reynolds Averaged Navier Stokes
SM	Service Module
SOAR	Single Stage Operational Assessment of Red Kite
φ	Equivalence Ratio

1. Introduction

1.1. Motivation

Current supersonic and hypersonic flight is achieved by rocket propulsion systems. Even though they are a reliable propulsion system, they come with several downsides, of which the most critical are the large fuel consumption due to the need of carrying oxidizer onboard. An alternative concept is air-breathing propulsion, which uses the atmospheric air as oxidizer, which leads to a significant reduction of onboard fuel or an extension of the range of the vehicle. Even though the basic concept is quite simple the realization of afore mentioned propulsions comes with technological challenges and currently several concepts are under investigation. The most technologically advanced systems are ramjets and, to a certain extent, scramjets which compress incoming air solely by accumulation effect and subsequently burn the fuel with the compressed air at subsonic (ramjet) or supersonic (scramjet) speed. The APEX-TD flight was set-up to verify numerical simulations and close the gap between wind tunnel experiments and cost intensive supersonic speed tests under real flight conditions. Additionally, critical components for advanced supersonic propulsions were designed, tested and verified.

Main challenge of the APEX-TD flight experiment was the limited time frame of less than 12 month from conceptual design in January 2023 to flight on November 13, 2023 and resource scarcity. Within this 10-month period, basic design, manufacturing, avionics testing and environmental tests were performed. In order to meet the deadline, an agile and pragmatic experimental set-up was chosen. The main differences to conventional flight experiments were a small core team and reduced review cycles allowing design and manufacturing in parallel and adaptation of the experimental setup during the whole development phase. Additionally, the experiment benefited from other flight experiments and wind tunnel experiments at the DLR allowing pragmatic decision making on empirical basis rather through extensive scientific investigations and numerical analysis.

1.2. State of the Art

Several flight experiments on supersonic combustion engines technologies have been performed in the resent years all over the world. Some notables are the Russian lead Kholod flight experiments in the beginning of the 90s [6], the Australian HyShot [4] and following HiFire [5] program, as well as the American X-43 [7] in the beginning 2000. In the last decade more flight ready projects were brought to live like the American X-51 or the Russian SS-N-33 Zirkon.
In Germany the supersonic and hypersonic flight experience by the DLR was focused on thermal and structural aspects as well as fundamental aerodynamic and aerothermodynamic and resulted in multiple flight experiments like the SHEFEX [8], SHEFEX II [9], ROTEX-T [10] and STORT [11] (see Figure 1).

Figure 1. Timeline of hypersonic flight experiments of the DLR

Long-term research on hypersonic air-breathing propulsion at the DLR was explicitly performed in the recent decade within Research Training Group 1095/2: "Aero-Thermodynamic Design of a Scramjet Propulsion System" of the German Research Foundation (DFG) [3] and the ITEM-FK and FK2020+ project as well as within the European HEXAFLY-INT project [12] and its precursor projects. One direct precursor of the APEX-TD configuration was the LK4 configuration of an axial-symmetric inlet for a generic Ramjet developed within the ITEM-FK project which was intensively investigated numerically and experimentally and was adopted to supersonic operation for APEX-TD. In Figure 2 the physical model is shown with (nearly) closed and opened inlet. Especially the experience with this wind tunnel tests performed at the TMK of the DLR Cologne allowed the implementation of the active opening mechanism into the physical flight experiment without intensive additional numerical investigations and wind tunnel tests.

Figure 2. Wind tunnel model of the LK4 configuration of the ITEM-FK project

2. Launch Vehicle Configuration and Trajectory

The launcher of the APEX-TD flight experiment was a single-stage Red Kite sounding rocket. In fact, the flight was conducted as a passenger experiment of the SOAR (Single-stage Operational Assessment of Red Kite) mission which performed the inauguration and qualification flight of the given motor. The rocket motor is solid propellant in the 1t class with a relative short burning time of less than 13 seconds and is described in detail by Scheuerpflug [2]. The vehicle including the experiment was approximately 6.6 m in length with an overall lift-off mass of 1570 kg, of which the payload was approximately 250 kg.

In Figure 3 the configuration of the launch vehicle is shown with the main components. APEX-TD was the payload of the SOAR flight and was mounted on the tip of the launch vehicle. The details of the payload are described in detail in the following chapters while the launcher and the flight are documented by Röhr [1].

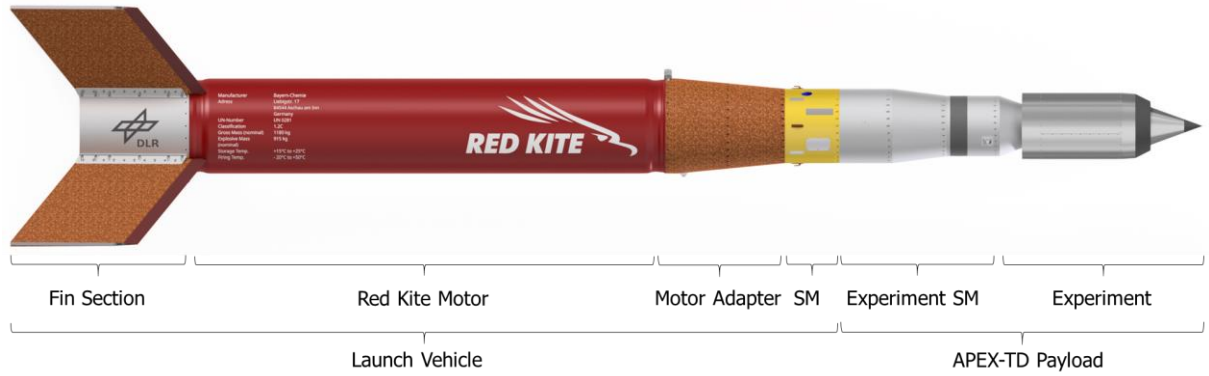

Figure 3. Configuration of the Rocket Motor

A main constraint of the APEX-TD flight experiment was to guarantee arrange with the schedule and requirements of the qualification of the rocket motor. Therefore, the trajectory was primarily driven by flight safety considerations. A ballistic flight trajectory with some 80° launch elevation, passive aerodynamic spin-up, no de-spin and without payload recovery was chosen, thus keeping overall system

complexity to the necessary minimum. A major difference to comparable experiment was to use explicitly the ascent phase of the flight as the major experimental phase due to the following reasons:

- Higher speed since the accumulated drag significantly decreases the velocity during the descent in comparison to the ascent
- More practical relevant mode transition from solid booster to air-breathing mode
- Additional measurements still possible during descent
- Simple and reliable fuel injection mechanism

The trajectory itself was split into three phases where the experimental phase was again split into three subphases:

1. Booster Phase
2. Primary Experimental Phase (during ascent)
    a. Inlet Opening Phase
    b. Stationary Flight Phase
    c. Fuel Injection Phase
3. High Altitude Flight Phase
4. Re-entry Phase

In Figure 4 the flown trajectory derived from the onboard GPS signal is shown with a closeup of the ascent (solid line) on the right indicating the different experimental phases. The peak velocity of Mach 4.8 was reached in in 9.8 km altitude, inlet opening started at Mach 4.6 and 12.1 km altitude and injection was started at Mach 4.0 and 17 km. For comparison the descent is shown as dashed line as well and indicated significant decreased velocities. The vehicle reached an apogee of 71 km and a maximal Mach number of 3.4 during descent at 20 km. These performances were slightly smaller than expected from the pre-flight simulations. Splash-down of the rocket was 58 km from the Norwegian coast line. A detailed recapitulation of the trajectory and Red Kite flight qualification is given by Röhr [1].

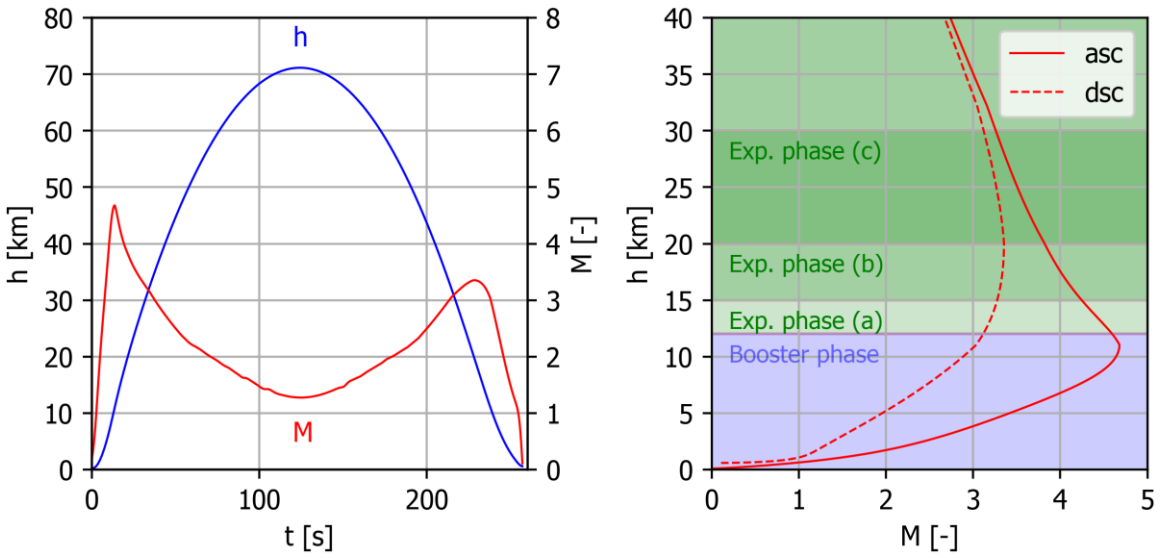

Figure 4. Trajectory of the APEX-TD flight experiment

2.1. Flight Stability and AEDB

A major concern during the experiment design was the flight stability. Due to its unusual shape in comparison to conventional sounding rocket payloads and the internal flow a conservative static stability margin of two calibres was requested. Multiple design iterations and detailed numerical simulations were required to achieve the requested stability. In Figure 5 the centre of pressure (x_{cp}) and centre of gravity (x_{cog}) are shown for different iteration steps and indicates a critical phase at the predicted maximum Mach number of 5 where the centre of gravity including the requested margins closely overlaps the preliminary numerical Euler simulations for the closed inlet configuration. By increasing

the fidelity of the numerical simulations from Euler to RANS, the expected centre of pressure was shifted backwards. Additionally, the performance loss due to higher experimental mass combined with slightly adjustments in centre of gravity finally ensured stability throughout the whole domain. Also, the high-fidelity simulations of the configuration with opened inlet have been performed and showed that the centre of pressure moves upstream and destabilize the vehicle but was above the two-calibre limit for the whole domain.

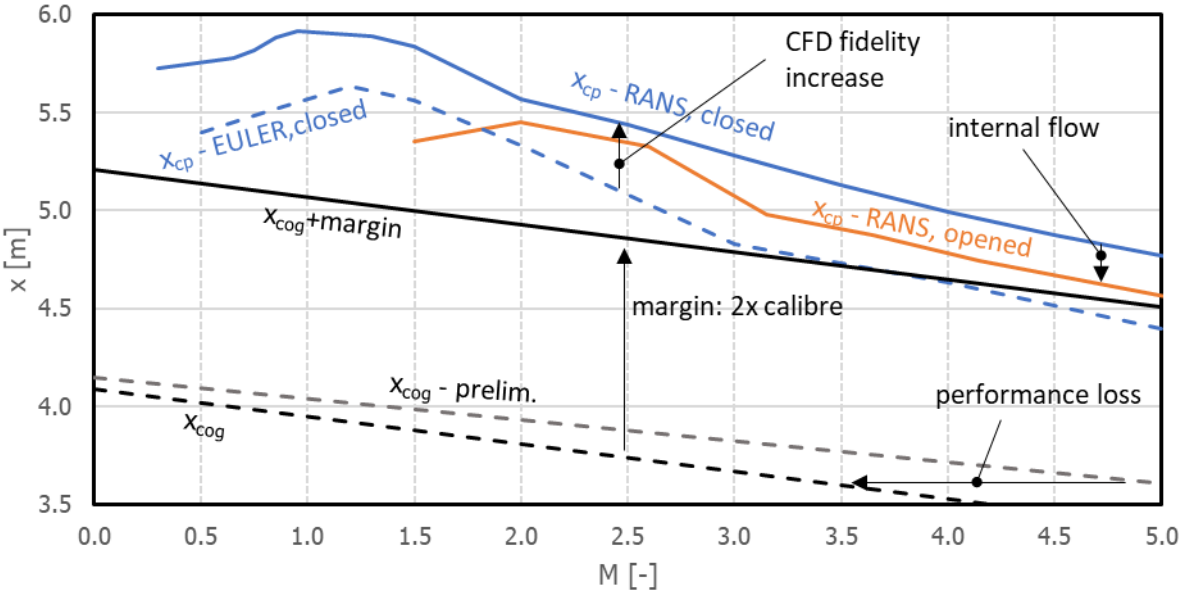

Figure 5. Static vehicle stability with margins

Additional to the stability analysis the numerical simulations were used to create an aerodynamic database (AEDB) which was used for calculating the flight trajectory. The Reynolds-Averaged Navier-Stokes (RANS) simulations have been carried out with the DLR-TAU Code. TAU is a hybrid structured / unstructured finite volume flow solver based on the compressible Reynolds-Averaged Navier-Stokes equations. For the current study steady simulations with a second-order upwind spatial discretization scheme have been performed. The Spalart-Allmaras one-equation turbulence-model was used to closure the system of equations. For comparison also Menter's shear stress transport model was applied. A fully turbulent boundary layer was assumed for all altitudes and Mach numbers investigated. Simulations have been performed for the open, closed and intermediate state of the hypersonic experiment with a computational mesh size of about 60 million degrees of freedom.

3. Experimental Design

The APEX-TD flight experiment was defined to cover several aspects of supersonic propulsion, except actual combustion processes. Hereby the focus was on technology demonstration as well as scientific investigation and reference data collection for comparison and validation of numerical simulations and wind tunnel test. This chapter gives a general overview on the design and technical realization of the experiment. In the following chapter different experimental aspects are descripted in detail together with some preliminary findings and evaluations.

3.1. Reference Configuration

The experiment was adapted to the rocket motor Red Kite and sized for a scramjet engine operating at low Mach numbers with supersonic internal flow at speeds down to a free stream Mach number of 3. Preliminary performance indicated a maximal Mach number of 6 but was later corrected to 5. A higher margin for stability as well as an increased experiment diameter of 390 mm for sensor accommodation lead to more mass and higher drag resulting in that performance loss. To get maximum stability a rotational-symmetric geometry was chosen, which significantly simplified preliminary numerical investigations and stability calculations. Additionally, this configuration allows a mechanism for closing the inlet during the boost phase which is descripted in the next section. As descripted in

chapter 2 and in Figure 4 the main experimental phase was between 13 and 40 km at Mach number ranges from 4.8 down to 2.8 and also allow operations during descent flight phase.

The upper part of Figure 6 shows the reference geometry of the experimental section and thereby the main scientific focus of the vehicle. The blue line indicates the inner contour which was used as main support structure. The inner contour was surrounded by a ring-shaped outer shell which is shown as a green line. In order to fix the outer shell to the inner contour six struts where mounted circumferential and are also shown in the figure in grey between the both other shapes and also in Figure 8. Also, the closed inlet configuration is shown with blue dotted lines. Hereby the inner contour and the outer contour are nearly close at the tip of the outer ring leaving only a narrow slit with a revolving gap of less than 0.5 mm. The mechanism and inlet are descripted in detail in 3.2 and 3.4.

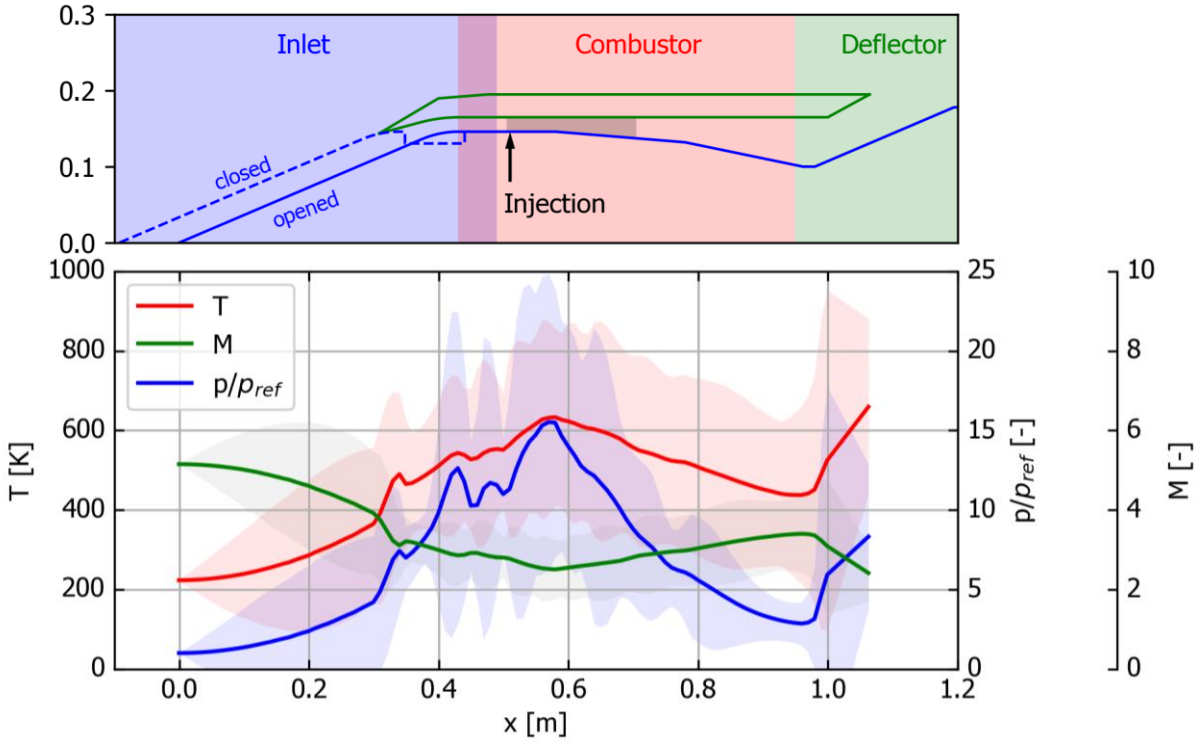

Figure 6. Reference geometry of inlet and flow properties of internal flow path.

Functional the three main section inlet (blue), combustor (red) and deflector (green) are also shown together with location of gas injection as a black arrow. The inlet is used to compress the flow and provide conditions for combustion in the combustor. In the combustor the fuel is injected, mixed with the incoming air and burned whereas the flow is slightly expanded to avoid thermal choking. The expansion angles are 4° and 10° resulting in a geometric expansion of ~1.7 and ~2.9 with respect to the combustor entrance. The six struts which hold the outer ring are used for an additional internal compression (geometric factor 1.14) and as shock generators for ignition triggering. The overlap between the inlet and combustor is the isolator and is not explicitly defined and is roughly 7 cm long. The deflector in the rear part of the experiment is not a major scientific part of the experiment, since it only releases the internal flow back into the surrounding flow, but is very crucial since it can cause blockage of the internal flow and inherit a critical risk on the whole experiment.

In the lower part of Figure 6 the mean values including the 2-σ standard derivation of the key flow parameters of a pre-flight simulation at Mach 5.15 without injection and combustion is plotted. It can be seen, that Mach number is decelerated to a minimum of 2.5 resulting in a temperature increase up to ~630 K and a pressure rise by a factor of ~16. Especially the temperature of 630 K is quite low and may be too low to ensure ignition, but considering the inhomogeneity of the flow temperatures of up to ~880 K can be reached at local hot spots. Also visible is that the compression is not only achieved by the inlet alone, but also by the struts which contribute approximately 20%.

Since no reactive fuel was used with no actual combustion this represents the reference configuration, no deep analysis on the combustion process was performed. Also, the configuration was not designed

as an operational engine and no analysis to applications for real flight engines were performed during the design process.

3.2. Inlet Design

The core element of the experiment was an axial symmetric inlet with a geometric compression ratio of 3.5 designed for Mach numbers up to 6. The ramp angle was set to 20°. Since self-starting of the inlet is not expected for the whole flight trajectory and in order to avoid negative effects on the propelled flight phase during ascent a mechanism was foreseen to close the inlet for the initial 15 seconds of the flight.

The inlet itself was derived from an inlet developed for ramjet mode, but was adapted to allow full supersonic flow through the whole internal duct. This was mainly achieved by reducing the internal expansion with no expected flow separation and no artificial applied back-pressure rise. Since the precursor model was tested in the TMK blow down wind tunnel for Mach numbers between 2.0 and 4.5 a high confidence in a reliable operation of the inlet was gained. Both, the wind tunnel model and the flight experiment were equipped with a movable front cone which allow closing of the internal flow duct and due to the wind tunnel experiments a high confidence in the principle starting mechanism was existent. In Figure 7 the Kantrowitz and isentropic compression ratio as well as a modified self-starting formulation [15] is shown for different free stream Mach numbers whereas the lines were scaled to the Mach number at the lip (or resp. beginning of internal contraction). The green area shows the range in which the internal contraction can be changed and ranged from $1/CR_i = 0.77$ for fully opened inlet to 1.0 for fully closed. In general, the inlet is very robust designed due to the relatively low internal contraction ratio and would self-start even during the whole flight above Mach 2.0 even if a sudden blockage would be occurred during flight.

A pneumatic mechanism was chosen to perform the opening of the inlet for the flight using a single centrical double-acting pneumatic cylinder which was extended when the inlet was closed. By simultaneous pressurization of one side and depressurization of the other side the inlet cone was moved between open and closed configuration. During the actual flight experiment the state of the inlet was only changed a single time from closed to open.

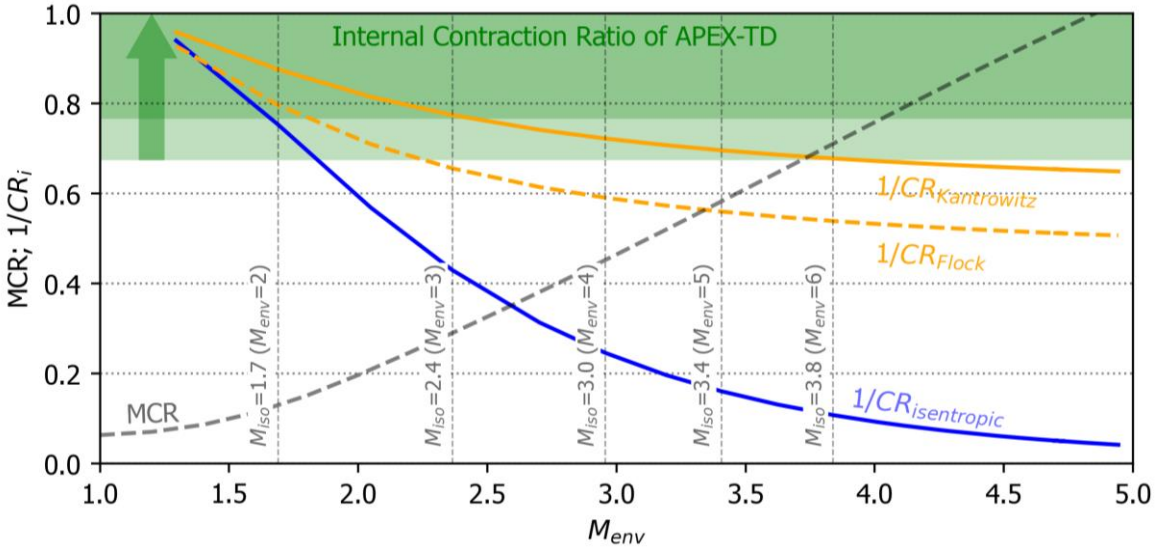

Figure 7. Internal contraction ratio of the APEX-TD inlet

3.3. Mechanical Layout

In Figure 8 a longitudinal cut through the APEX-TD vehicle is shown with some major components of the experiment, hereby the image is not in the final flight configuration since some changes in the pressure and data acquisition module were adapted in later states of the development.

In principle the experiment was separated in a front experimental module which consist of the inlet, the internal flow path and a flow deflector. After this module the signal conditioning and after this the pressure and data acquisition module followed. The experimental module was housing the different experiments, which are explained in detail in the next chapter, the sensors and the fundamental

mechanics to allow an operation of the experiments. The signal conditioner box collects all sensor signals and provided the individual sensors with the required power and mainly was used for cable routing and cable management. Finally, the pressure and DAQ module was used to control the pneumatic system in order to open and close the inlet as well as injecting gas into the combustion chamber. Additionally, it was used to digitalize and stream the sensor data in a serial data stream for the transmission to ground. In order to keep the logic within the vehicle at a low level to ensure save all operations were timeline driven with the lift-off as reference and commands provided by the rocket motor service module.

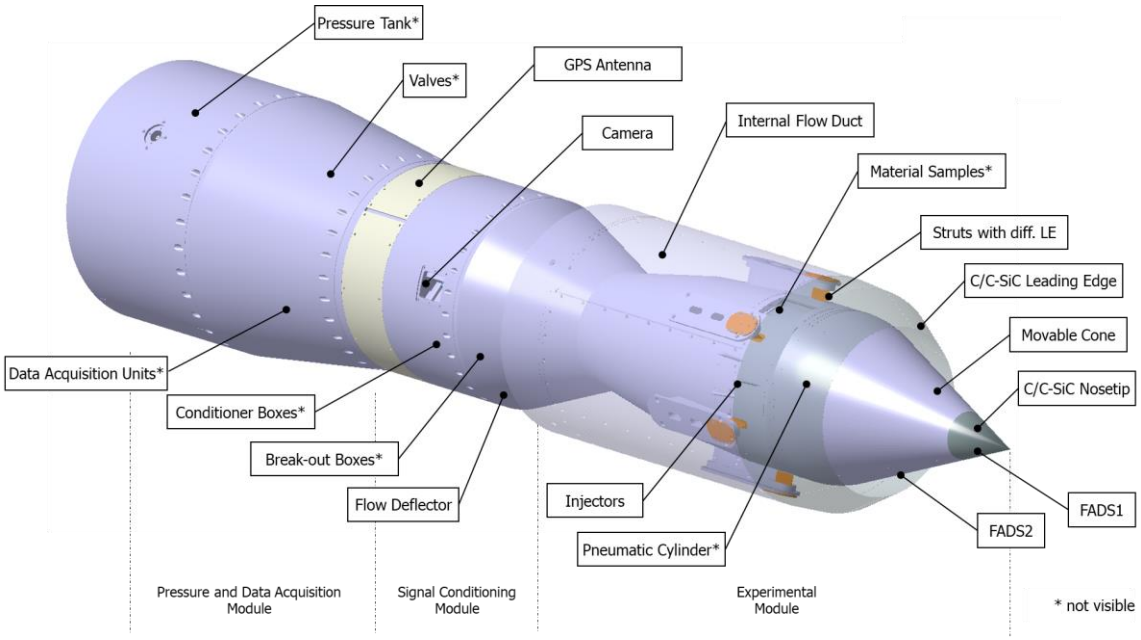

Figure 8. Schematics of the APEX-TD experiment

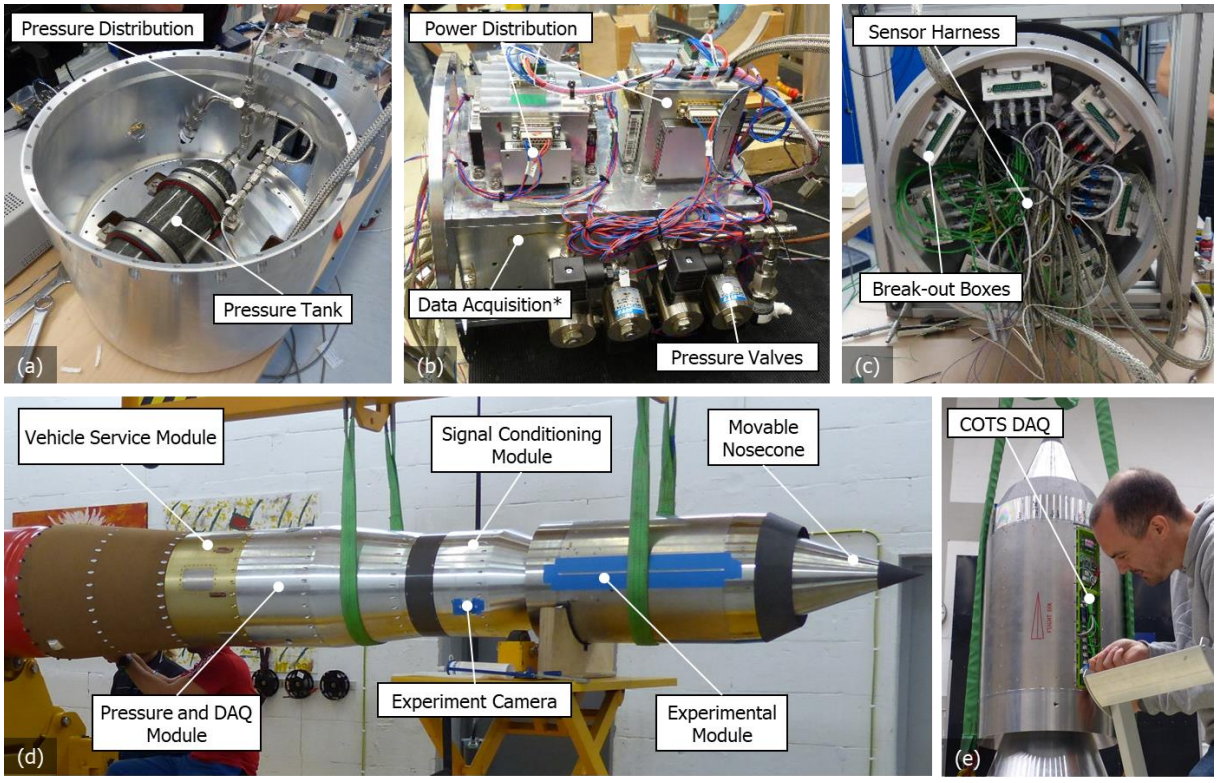

Figure 9. Picture of the experiment during the integration

In Figure 9 the different stages of the APEX-TD experiment are shown with major vehicle components. In comparison to Figure 8 changes are obvious especially in the pressure and DAQ module, because some design changes had been integrated quite late in the project phase and were not fully integrated into the CAD model.

3.4. Pneumatic System

The pneumatic system was critical because it was essential to provide save operations. For SOAR it had to keep the inlet closed for the booster phase while for APEX-TD it needed to be opened in order to ensure the operations of all experiments mentioned in the next chapter. Therefore, the system was designed as simple as possible and is shown in Figure 10. It consists of a pneumatic cylinder which was controlled by four valves, a pressure vessel with a volume of 2 l a filling block and a remote system de-pressure valve which was also used as injection system for the experiment. The cylinder is directly connected to the inlet cone and opens or close the inlet. Due to the use of the normally closed valves the operation of the vehicle was quite reliable, as the state of the vehicle was kept in case of an unexpected power off mode and even would have worked under partial malfunction of some valves. The system could be remotely depressurized via the injection system or manually via a valve in the filling system.

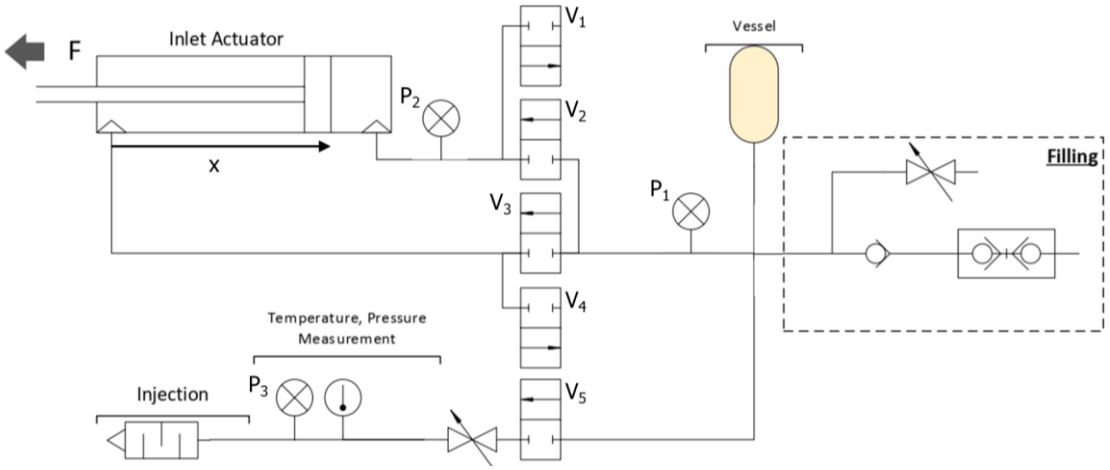

Figure 10. Pneumatic system of APEX-TD

In Figure 11 several pressure system key parameters recorded during the flight are shown and indicate the major events during the experiment. At around 14.3 s the valves 1 and 3 are opened and as soon as the pressure difference (including the external aerodynamic forces) between both sides on the cylinder inverts the cylinder is moving and starts the opening of the inlet which roughly begins at 15 s and end at 15.9 s. For further 1.5 s the valves are held open until closed and lock the inlet in place. At 19 s the residual pressure in the tank is release by opening the valve 5 thru the injection system until the residual pressure in the system is around 2 bar 60 s later.

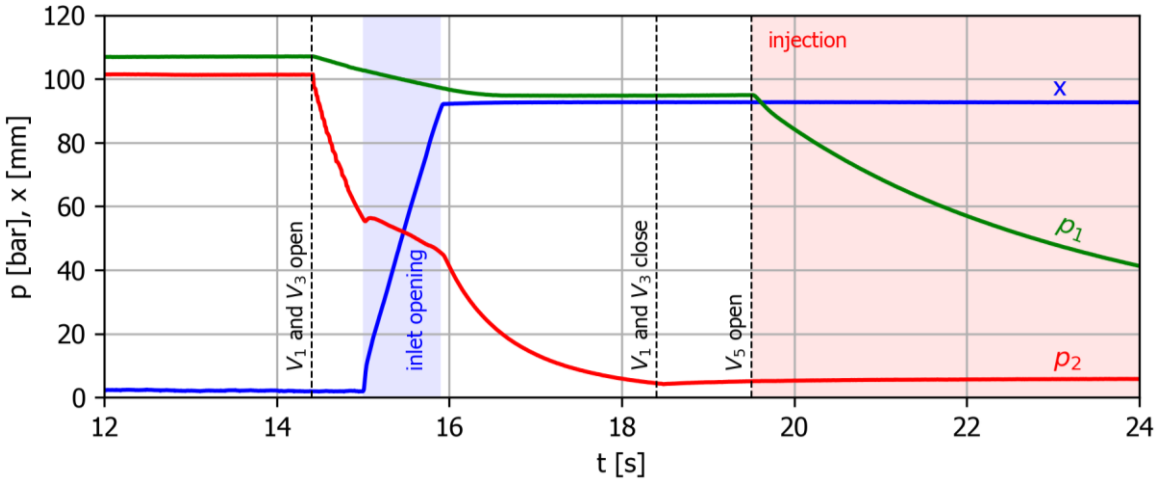

Figure 11. Timeline of the pneumatic system during flight

3.5. Instrumentation

The main focus of the experiment was to gather extensive flight data for supersonic and hypersonic flight. Therefore APEX-TD was equipped with two separate main data acquisition systems collecting data of approximately 140 sensors with data rates of up to 2500 Hz. Hereby the following main aerodynamic and aerothermodynamic sensor types have been used:

- 45 pressure sensors
- 32 surface thermocouples (heat flux)
- 56 structural thermoelements

Additionally, a low-cost COTS data acquisition with several COTS pressure sensors and further internal housekeeping data was integrated (see Figure 9.e) into the vehicle, but due to a defective UART/RS422 interface converter not able to communicate with the system bus and therefore had to be disabled for the flight.

The goal was to receive measurements for comparison with numerical simulations, wind tunnel data and analytic predictions. Beside the general flow topology, the focus was to verify the experimental aspects descripted in the following chapter. As it can be seen in previous pictures (Figure 8 and Figure 9) the design and manufacturing of the experimental section was broadly driven by the data acquisition and integration and accommodation of the sensors and the supporting equipment.

For reliability and simplicity, the data acquisition system was designed to operate in continuous operation mode and to acquire and process sensor data as soon as power was provided by the service module without specific commands. Figure 12 shows the data acquisition concept. It depicts the flow chart of the sensor data through the data acquisition system. Sensor data is collected by the sensors and each sensor is connected to one of seven break-out boxes (BOB's). These boxes bundled the sensor cables and connect it to the conditioning boxes (COND), which amplify the data and also provide power if needed to the specific sensors. Than the signals are forwarded to the data acquisition cards of the data acquisition boxes (DAQ) which digitalized the sensor data and packed it into serial data frames. Than the data frames are packed into a serial data stream and transmitted via UDP (DAQ1) and RS422 (DAQ2) to the vehicle service module via two separate data interfaces and transmitted to ground via the vehicle service module.

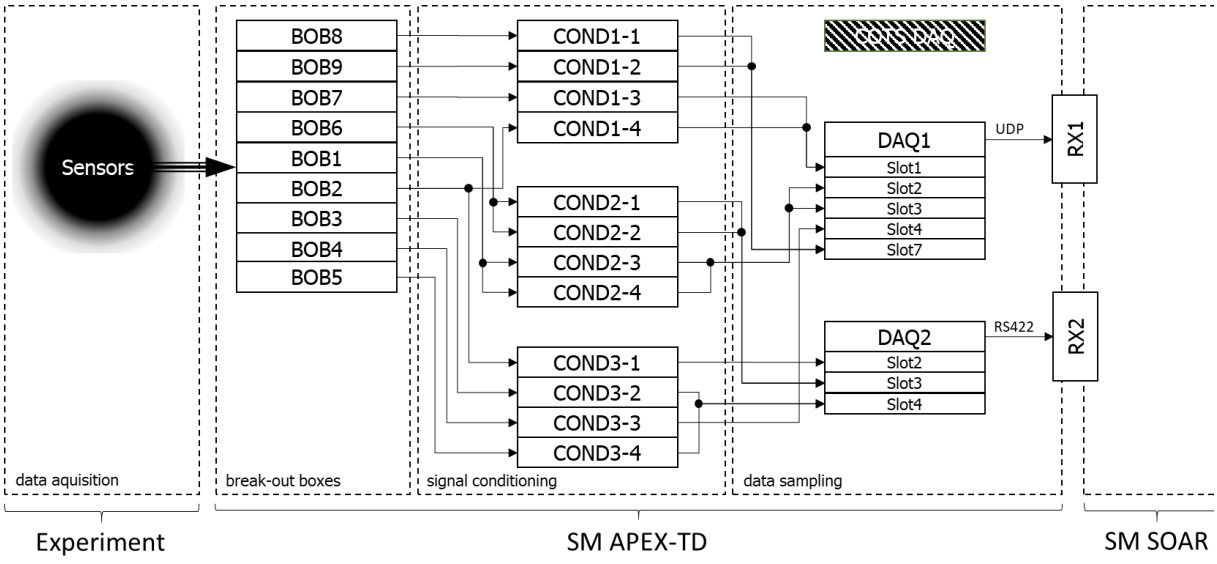

Figure 12. Data acquisition flow chart for APEX-TD

A data rate restriction for downlink of the experimental data was given by the two data interfaces to the vehicle service module, which restricted the rate to a maximum of approximately 2.5 Mbit/s (316 kBytes/s) for the whole APEX-TD experiment. In order to fit the different sensor data into the bandwidth different sampling rates between high, medium and low was chosen for each system and sensors were assigned according to their required data rate. In Table 1 the sampling rates and the theoretical data rate are shown.

During the actual flight the data rate was slightly higher due to header and synchronization data. On the other hand, electric noise generated sporadic bit errors on the RS422 signal which caused a package lost from the RS422 data stream which caused a data loss between 3-10% on this data stream depending on the data reconstruction method. Beside these onboard data noise, no significant data loss was observed and data was gathered until approximately 330 m before impact. Since both data acquisition systems where run parallel synchronization of both timelines where performed by measuring the same onboard binary lift-off signal with both data acquisition systems.

Table 1. Sampling and data rates of the different data acquisition streams

	Channels *[-]*	**Sampling rate** *[Hz]*	**Data rate** *[kByte/s]*
DAQ 1 (UDP)	**135**		**218.5**
Low Speed (LS)	89	250	44.5
Medium Speed (MS)	28	1500	84.0
High Speed (HS)	18	2500	90.0
DAQ 2 (RS422)	**98**		**97.0**
Low Speed (LS)	72	240	34.6
High Speed (HS)	26	1200	62.4
Total	**233**		**315.5**

In addition to the scientific data visual video streams were gathered via two cameras. One was used for visuals of the rocket motor in the frame of SOAR and one for the observation of the APEX-TD experiment. In Figure 9 the location on the vehicle of the experimental camera is shown whereas in Figure 13 the close-up with a sketch of the field of view (yellow, left) as well as the actual field of view during the final seconds of the re-entry is shown (right).

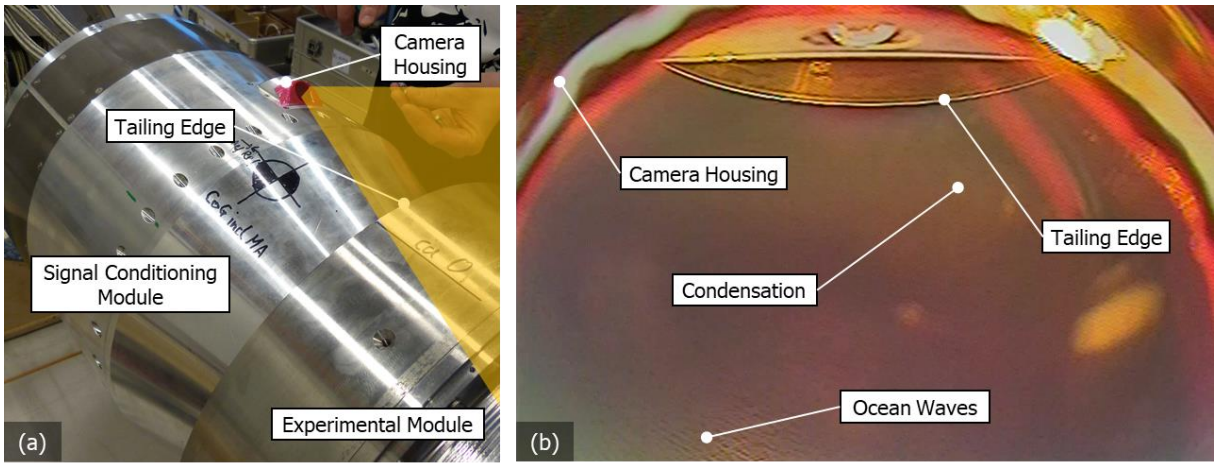

Figure 13. Close-up of camera location and field of view during descent flight

Additional data has been obtained from the vehicle service module, namely GPS and IMU data, as well as from weather balloons prior to flight.

4. Experiments

Only a minor selection of the data of the experiment will be shown in this chapter to give a first look on the experimental results. A detailed analysis of the results will be presented in upcoming investigations. The data are not in their final form and do not include all corrections like temperature compensation and may change in further investigations. Of note is the use of the 1976 standard atmospheric model which was not corrected by balloon measurements and therefore no adaption to launch side conditions were performed.

4.1. Inlet Starting and Characterization

The inlet operated as it was expected from the design phase. In Figure 14 the pressure of a selection of sensors in the inlet normalized by the atmospheric pressure is shown. It shows that the inlet is closed during the first 15 seconds of the flight since the internal pressures are significantly lower than the pressure in the ramp (orange). An exception is the red line, which is from a sensor located precisely on the slit when the inlet is closed. Since the gap is not totally closed the fluctuation are a very small and a local phenomenon. With the opening of the inlet the flow changes and the pressure inside rises by the factor of up to 15. Surprisingly it is not instantly and occurs with a delay of approximately 1 second. A more profound investigation shows that this delay occurs only on the bottom side and indicates the presence of a separation region which is dissipated slowly with flight time. After 2 seconds the flow in the internal part is fully established and quite constant for up to second 28, where it starts to oscillate which seems to be a phenomenon originated from the back of the internal flow duct.

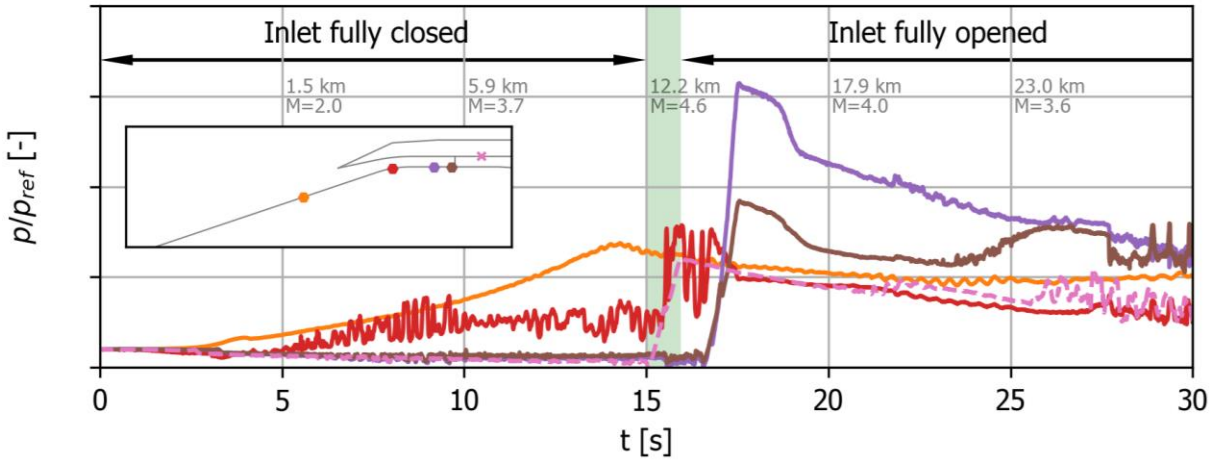

Figure 14. Normalized pressure plots of inlet operation during ascent

During the re-entry the behaviour was completely different and is shown in Figure 15. A significant oscillation is visual at 230 s which decreases and nearly disappear at 235s. It's most likely due to the increased angle of attack oscillation during re-entry which propagates downstream. At 13.1 km and Mach 3.2 a sudden increase in pressure is observed which correlates with a high frequency oscillation and can be explained with a blockage of the inlet and so-called "inlet buzzing". This oscillation propagates very far upstream and is even visible at 350 mm (orange sensor). During the buzzing several sensors exceed their limits (red, blue and pink) and one even breaks (brown). The reason for the buzzing was not expected at this Mach number and it needs to be investigated further.

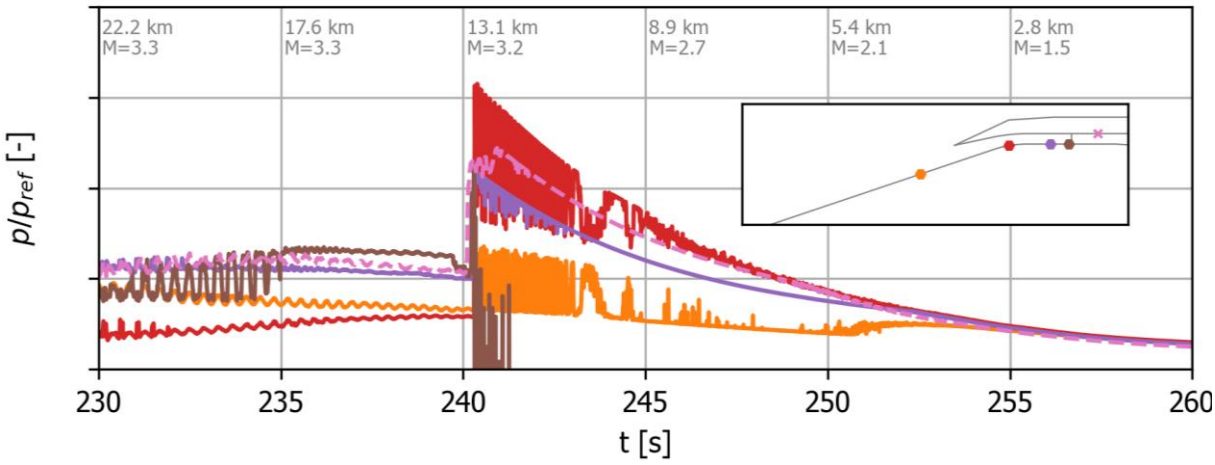

Figure 15. Normalized pressure plots of inlet operation during descent

In general, all aspects predicted during the design phase of the inlet have been observed, but during a detailed investigation some discrepancies occurred and need to be investigated in detail. Also, not all

sensor data has been investigated yet and needs to be corrected for temperature effects and data integrity before allowing final conclusion on the inlet behaviour.

4.2. Internal Flow Structures

The internal flow structures are strongly connected to the inlet characterization as the flow structures generated in the inlet are propagated thru the internal duct. With this propagation small changes accumulate and have an "butterfly effect" on the general flow and in particular to the supersonic shock structures. Figure 16 the normalized pressure distribution on the lower and upper wall of the internal duct is shown. Hereby the CFD was performed for a preliminary trajectory with Mach 4.15 at an altitude of 20 km while during the flight Mach 4.15 was reached earlier in 15.7 km altitude at 18 seconds after lift-off. For the comparison the pressure was normalized by the environmental pressure and match within a reasonable range between both data source. The amount of pressure sensors of the experiment is to low to resolve the flow and shock structures within the combustor directly but matches the peaks and valleys of the numerical simulations. Some differences are seen and cannot be explained at the current state and further investigations need to be performed. Reasons may be slightly angle of attack of the vehicle during the flight, boundary layer effects, influence of wall temperature, atmospheric composition or other influences. A detailed analysis is needed which requires a better reconstruction of the trajectory and atmosphere as well as numerical simulations for specific flight conditions along the actual flight profile.

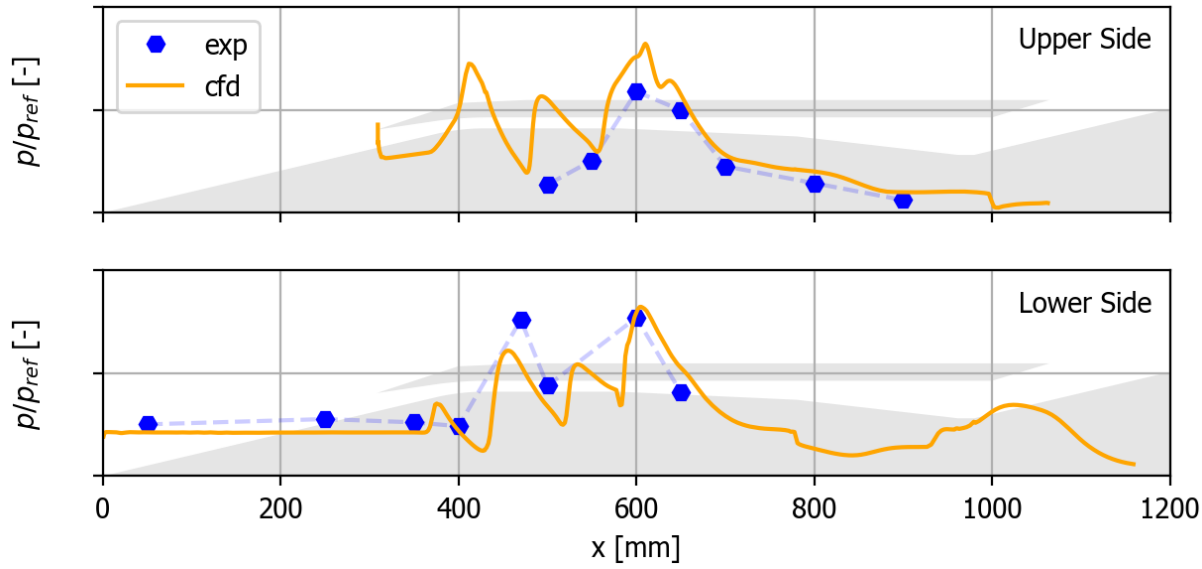

Figure 16. Pressure distribution from experiment and CFD at Mach 4.15 on the upper and lower wall.

4.3. Ceramic Structures

Entropy boundary layers play an important role in supersonic inlets, especially in small scale experimental vehicles. For practical vehicles the effective leading edges sharpness is usually restricted either due to manufactural reasons or due to material degeneration under harsh environments. These blunt leading edges cause a high pressure loss in the boundary layer. This boundary layer is usually swallowed downstream of the leading edges into the combustor and decreases the performance of the combustion process. Reducing this effect is possible via boundary layer suction or by using sharp leading edges. In this experiment the second option was investigated by using high temperature C/C-SiC ceramics. Hereby the tip of the nose, the radial leading edge, and the tip of two struts were equipped with these ceramics, whereby the edges were manufactured with technical sharp-edges (<0.05 mm). In Figure 17 the C/C-SiC components are shown. The goal of the experiment was to gather thermal data of these components under realistic flight conditions and investigate the form stability of the components via numerical analysis and comparison with the obtained data. For the C/C-SiC insert in the strut different alternative materials were used in the other four struts (copper, stainless steel, Inconel) which allow a direct comparison between of different materials under nearly identical conditions.

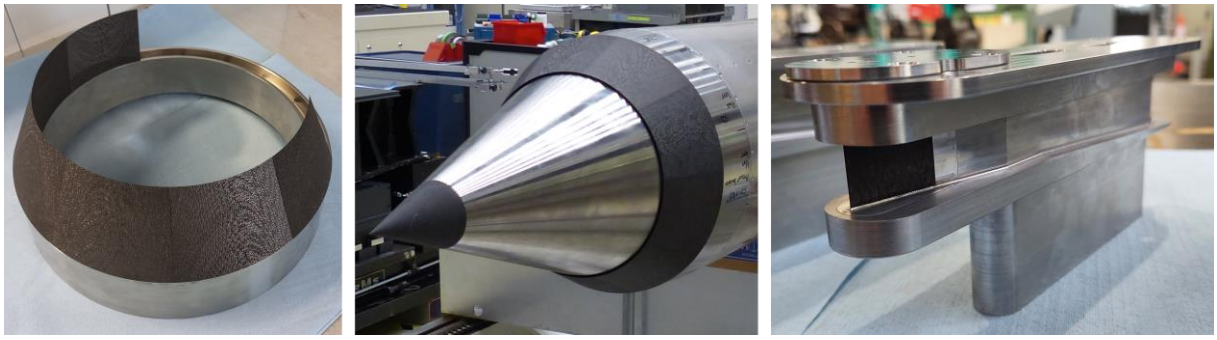

Figure 17. Sharp leading edges with C/C-SiC components

In Figure 18 the temperature evolution of the C/C-SiC nosecone and the leading edges of the struts are plotted for the ascent and the descent flight phase. In general, the temperatures are quite low in comparison to hypersonic experiments due to the low maximum flight Mach number. Nevertheless, the temperatures on the struts are still quite high reaching up to 500°C after around 21 seconds into flight and a very close the total flow temperature. Here the C/C-SiC struts show the most significant temperature rise. Interestingly the increase starts already when the inlet is closed, indicating a hot jet impinging on these struts. As soon as the inlet is opened the flow changes which results in an unexpected decrease in temperature on these strut temperature measurements. A similar effect occurs on the stainless-steel strut which reaches comparable temperatures. What specifically is the reason for this behaviour needs to be investigated in detail and require detailed CFD and FEM simulations. The copper strut shows significant lower temperatures reaching only 140°C which is caused by the higher heat conductivity. General this arrangement allowed a direct comparison of different materials under similar conditions and are well suited for further numerical analysis and comparison and extrapolation for actual applications in scramjet engines.
In the lower graphs of Figure 18 the temperature of the nosecone is shown at different depths. A maximum of 360°C is reached at the most upfront sensor during ascent. During descent the temperatures are changing marginally indicating no significant heating on the nose.

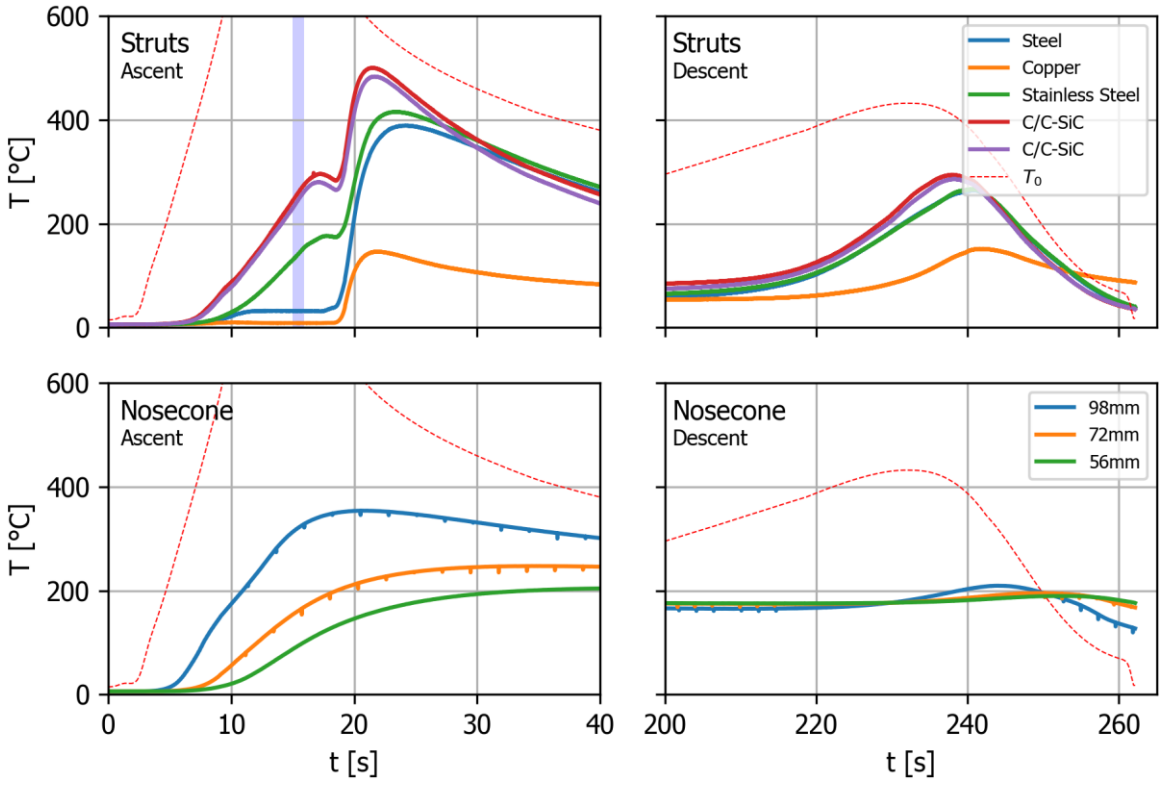

Figure 18. Temperature evolution of struts and C/C-SiC nosecone during ascent and descent

4.4. Fuel Injection and Regenerative Injector Cooling

The injection of a fuel equivalent was an optional goal for the flight experiment and was integrated quite late in the design process. Due to security and qualification concerns in combination with the tight schedule actual injection of reactive gases like hydrogen or methane was only investigated theoretically and used for reference calculations. For the real flight non-reactive nitrogen was used.

Since the injection of the nitrogen was during the ascent and was feed by a pressure tank no complex fuel flow control was needed. In order to keep a constant fuel to air ratio for the injection during the ascent the fuel mass flow and hence the pressure of the fuel reservoir has to decline exponentially due to exponential atmospheric pressure distribution. Simultaneously the fuel tank pressure declines exponentially while it depletes and hence decreases the fuel mass flow rate exponentially as well. By adapting fuel tank size, initial pressure and valve settings the mass flow from the tank can be adapted to the mass flow requirements for the specific trajectory.

In Figure 19 the theoretically required stoichiometric mass flow of methane fuel for one chamber of the actual flight trajectory is plotted (dashed blue line). On the other hand, the actual fuel (respectively the nitrogen) mass flow derived from the pressure drop of the tank measurement is shown as solid blue line. By dividing both curves the equivalence fuel-air ratio (φ) is obtained and is nearly constant with a value of 0.5 for the first part of the fuel injection phase and later rise constantly up to 1.5 at 36 km altitude. The graph shows that the fuel system worked perfectly and this simple but robust system can be adapted for scramjet flight experiments. It has to be considered that the molar weight of nitrogen is nearly 2 times higher than of methane which implies that the volumetric stoichiometric ratio was very close to the ratio what would be expected during injection with methane.

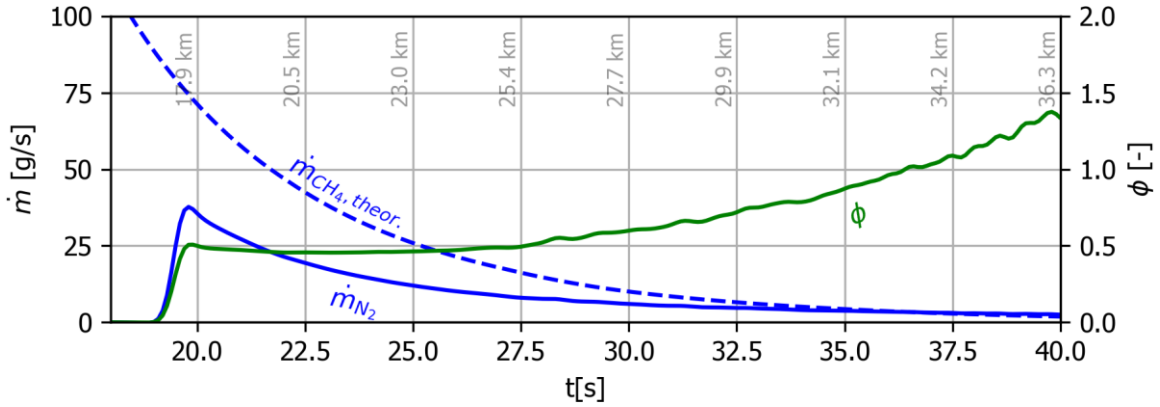

Figure 19. Fuel mass flow for APEX-TD

For the actual injection of the nitrogen into the core flow looped one-sided strut injectors with internal cooling and temperature measurement have been used. The design used the same basic concept developed within the frame of the GRK 1095 "Aero-Thermodynamic Design of a Scramjet Propulsion System" [3]. The injection was performed via four 0.75 mm injection holes on the rear of each injector with an inclination of 30° to the flow. Only one chamber of the experiment was equipped with a set of three injectors which were placed in an alternating pattern as it can be seen in Figure 20. The design was used to maximize mixing of the fuel and incoming air and also to create a shock pattern with local hot spots in the vicinity of the fuel injections for hypothetical ignition. Due to the small size and complex internal geometry metallic 3D printing has been used to manufacture the injectors and allowed short notice design changes and integration into the vehicle. The spare injector and a cross cut are shown in Figure 20.

Since inert gas was injected thru the injectors no actual combustion experiment could be performed. Although the conditions in the combustor are close to allow an ignition and combustion of an air-fuel mixture, it could not be verified experimentally or numerically of an ignition would be possible if actual fuel would have been used. So, the focus of this experiment was to verify the other effects of injection of a gas into the combustion chamber and gather data for comparison with post-flight analysis:

- Fuel mass flow control system

- Regenerative injector cooling
- 3D-printed injectors in supersonic flow
- Flow interaction of injectors and internal flow

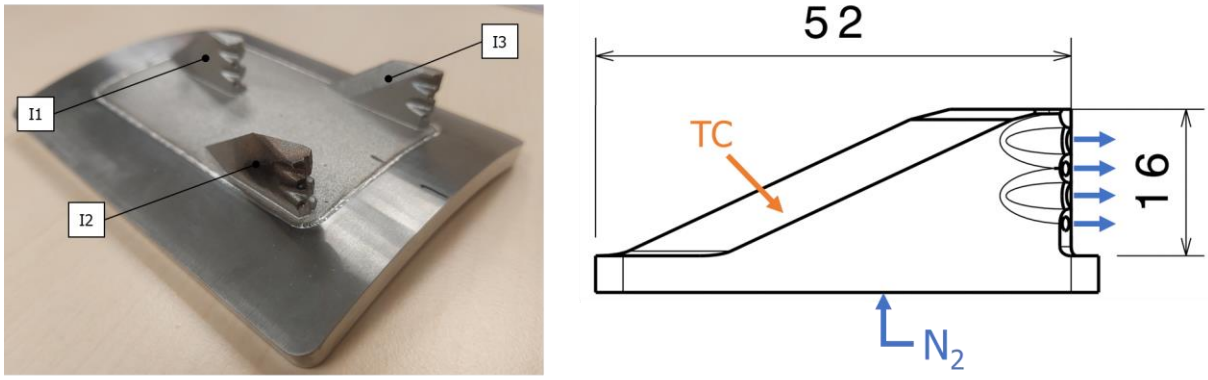

Figure 20. Sketch of the injector insert for the APEX-TD flight experiment

In Figure 21 the temperature of the three injectors are plotted during ascent and descent together. Since no direct comparison with an uncooled injector was foreseen the temperature of the steel strut was appended for comparison. The temperature of the three measurements are very comparable and for the descent also the reference temperature of the strut is very close to the others. Main differences are in the ascent phase. As long as the inlet is closed the injector is more heated than the strut. Also, as soon as the inlet opens the temperature increases drastically for the injectors while there is a certain delay for the strut measurement. The exact reason for this delay is unknown and was already discussed in 4.1 and needs to be investigated in detail in upcoming studies. Clearly visible is the start of the injection which cools the injector much more as the temperature decrease seen on the strut.

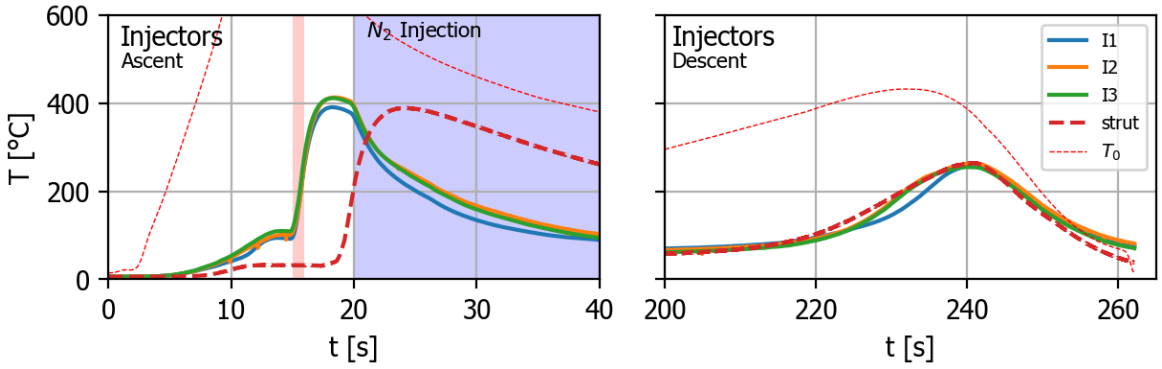

Figure 21. Temperature of the injectors during ascent and descent

4.5. Flush Air Data Sensing (FADS)

The concept of FADS was successfully tested and used in several other flight experiments and vehicles [13,14] and therefore also implemented into the current vehicle. The target of the system is to derive the free stream flow conditions like angle of attack, angle of roll, static pressure and Mach number of the vehicle by combination of several pressure measurements on the outer surface of the vehicle. The advantage over classical navigation systems is the flow state determination without drifting and atmospheric approximation as well as no need for external data like GPS signals. For this experiment two separate FADS were integrated which measured with four (every 90°) and six (every 60°) pressure sensors located circumferential around the nosecone of the vehicle. Also, since full data recording was performed for the flight a combination of both systems is also possible during postprocessing and is currently ongoing.

5. Summary and Outlook

The successful flight experiment APEX-TD launched in Andøya (Norway) on November 13, 2023 met all primary endpoints and also nearly all secondary mission goals. This paper describes main experiments

and their scientific focus as well as the technical aspects of the vehicle design. In addition, it presents first scientific results.

APEX-TD was a passenger experiment of the Red Kite flight qualification test. The main challenge for the project was the tight schedule with a time to flight of less than one year which was met due to minimal project management overhead and an agile and small project team. Minor failure was a low-cost COTS data acquisition system including pressure sensors and low-cost IMU where a protocol converter malfunctioned and could not be fixed in time.

Main systems, like the inlet and inlet opening mechanism worked as expected and showed results comparable to the predictions. Also, the successful fuel injection of a non-reactive gas indicated that an active combustion experiment would have worked and showed a reliable method of fuel injection for future scramjet experiments. Scientific data were collected from approximately 140 sensors for the whole flight trajectory and gathered nearly 100 Mbytes of sensor data for the 265 s long flight. First analysis presented in the paper showed reliable data which is in line with numerical and analytic predictions from the pre-flight design phase. Whereas some effects like inlet buzzing or inlet starting delay were not considered or expected for the flight experiment and needed further post-flight analysis.

As flight data evaluation and analysis just started, a detailed investigation of the experimental data is needed to understand anomalies detected during the flight. Also, data correction and data synthesis of the extensive data collection needs to be continued in order to get a more detailed picture of the flight experiment and subsequently understanding of supersonic and hypersonic flights order to be prepared for future missions and flight vehicles.

6. Acknowledgment

The authors want to thank the technical staff of Andøya Rocket Range, DLR Mobile Rocket Range (MORABA) and the DLR Department of Supersonic and Hypersonic Technologies for their support on performing the experiment as well as the DLR's Program Directorate for Security Research for funding this project.

References

1. T. Röhr, S. Scheuerpflug, J. Ettl, D. Kail, C. Mildenberger, J. Riehmer, C. Schnepf, R. Kirchhartz, Flight Qualification of the Red Kite Solid Rocket Motor. 3rd HiSST, 14 – 19 April 2024, Busan
2. Scheuerpflug, F., Röhr, T., Huber, T., Reinold, M., Hargarten, D., Kobow, L., Kirchhartz, R., Kuhn, M., Weigand, A., Berndl, M., Werneth, J.: The Red Kite Sounding Rocket Motor Qualification Milestones and Application Spectrum. 3rd HiSST, 14 – 19 April 2024, Busan
3. Weigand, Bernhard, and Uwe Gaisbauer. "An Overview on the Structure and Work of the DFG Research Training Group GRK 1095:" Aero-Thermodynamic Design of a Scramjet Propulsion System"." 16th AIAA/DLR/DGLR International Space Planes and Hypersonic Systems and Technologies Conference. 2009.
4. Smart, Michael K., Neal E. Hass, and Allan Paull. "Flight data analysis of the HyShot 2 scramjet flight experiment." AIAA journal 44.10 (2006): 2366-2375.
5. Dolvin, Douglas. "Hypersonic international flight research and experimentation (HIFiRE) fundamental science and technology development strategy." 15th AIAA international space planes and hypersonic systems and technologies conference. 2008.
6. Roudakov, Alexander, Vyacheslav Semenov, and John Hicks. "Recent flight test results of the joint CIAM-NASA Mach 6.5 scramjet flight program." 8th AIAA International Space Planes and Hypersonic Systems and Technologies Conference. 1998.
7. McClinton, Charles R., et al. "Preliminary X-43 flight test results." Acta Astronautica 57.2-8 (2005): 266-276.
8. Eggers, Thino, et al. "The hypersonic flight experiment SHEFEX." AIAA/CIRA 13th International Space Planes and Hypersonics Systems and Technologies Conference. 2005.

9. Weihs, Hendrik, J. Longo, and J. Turner. "The sharp edge flight experiment SHEFEX II, a mission overview and status." 15th AIAA International Space Planes and Hypersonic Systems and Technologies Conference. 2008.
10. Gülhan, Ali. "Main achievements of the rocket technology flight experiment ROTEX-T." 21st AIAA International Space Planes and Hypersonics Technologies Conference. 2017.
11. A. Gülhan, D. Hargarten, M. Zurkaulen, F. Klingenberg, F. Siebe, S. Willems, G. di Martino, T. Reimer; Selected Results of the Hypersonic Flight Experiment STORT, Acta Astronautica, Volume 211, October 2023, Pages 333-343
12. Steelant, Johan, et al. "Conceptual design of the high-speed propelled experimental flight test vehicle HEXAFLY." 20th AIAA international space planes and hypersonic systems and technologies conference. 2015.
13. Riehmer, Johannes, Ali Gülhan, and Johan Steelant. "Design of a Flush Air Data Sensing System for the Hypersonic Flight Experiment HEXAFLY-INT." (2022).
14. Thiele, Thomas, Ali Gülhan, and Herbert Olivier. "Instrumentation and aerothermal postflight analysis of the rocket technology flight experiment ROTEX-T." Journal of Spacecraft and Rockets 55.5 (2018): 1050-1073.
15. Flock, Andreas K., and Ali Gülhan. "Modified Kantrowitz starting criteria for mixed compression supersonic intakes." AIAA journal 57.5 (2019): 2011-2016.